Tang et al. *EPJ Quantum Technology* (2023) 10:50
https://doi.org/10.1140/epjqt/s40507-023-00207-9

EPJ.org
EPJ Quantum Technology
a SpringerOpen Journal

RESEARCH

Open Access

Demonstration of 75 km-fiber quantum clock synchronization in quantum entanglement distribution network

Bang-Ying Tang[1,2†], Ming Tian[1†], Huan Chen[4], Hui Han[3], Han Zhou[3], Si-Chen Li[3], Bo Xu[1], Rui-Fang Dong[5], Bo Liu[1*] and Wan-Rong Yu[3*]

*Correspondence:
liubo08@nudt.edu.cn;
wlyu@nudt.edu.cn
[1]College of Advanced Interdisciplinary Studies, National University of Defense Technology, Changsha, China
[3]College of Computer, National University of Defense Technology, Changsha, China
Full list of author information is available at the end of the article
[†]Equal contributors

Abstract

The quantum entanglement distribution network, serviced as the communication infrastructure which distributes quantum information among remote users, enables many applications beyond the reach of classical networks. Recently, the applications such as quantum key distribution and quantum secure direct communication, have been successfully demonstrated in the quantum entanglement distribution network. In this article, we propose a multi-user round-trip quantum clock synchronization (QCS) scheme in the quantum network, which can be implemented with one single entangled photon source located at the server. The server distributes the entangled photons to remote multiple users with the wavelength division multiplexing strategy, and each user feeds partial received photons back to the server. The clock difference between the server and each user is calculated from the one-way and round-trip propagation times, which are determined according to the time correlation of entangled photons. Afterwards, the demonstration has been conducted between the server and a user over a 75-km-long fiber link, where the measured clock difference uncertainty is 4.45 ps, and the time deviation is 426 fs with an average time of 4000 s. Furthermore, the proposed QCS scheme is linearly scalable to many users, with respect to user hardware and number of deployed fibers.

Keywords: Quantum entanglement distribution network; Quantum clock synchronization; Multi-user; Round-trip

1 Introduction

Quantum networks enable many applications beyond the reach of classical networks [1], such as information-theoretic-security communication [2, 3], high-precision quantum clock synchronization (QCS) [4, 5], distributed quantum computing [6], and distributed quantum sensing [7, 8]. Recently, quantum networks have already stepped into the entanglement distribution network stage [1, 9–14].

Quantum entanglement distribution networks have been successfully achieved by employing the wavelength division multiplexing (WDM) strategies to distribute entangled photons to distant multiple users in multiple degrees [13–17]. Currently, quantum key distribution [15, 16] and quantum secure direct communication [18] have been successfully demonstrated in quantum networks. Additionally, quantum entanglement distribution networks have the potential to implement multi-user QCS, facilitating high-security and high-precision clock synchronization for remote users [19–22]. The QCS scheme usually acquires the high-precision clock difference by calculating the time difference of entangled photons with the references of users' clocks, which avoids symmetric delay attacks inherently [23, 24]. Furthermore, the security of the QCS scheme can be evaluated by performing the Bell state measurement [22]. Currently, various point-to-point QCS schemes have been successfully demonstrated, including the two-way QCS scheme [23, 25], Hong-Ou-Mandel (HOM) interferometer-based QCS scheme [26, 27], and round-trip QCS scheme [24].

In the two-way QCS scheme, each user (Alice and Bob) has an entangled photon source, the idler photon is detected locally and the signal photon is sent through a fiber and detected on the remote side. The clock difference is calculated by applying an entangled photon cross-correlation algorithm and canceling out the photon propagation time [23, 28]. In 2022, Hong H. et al. demonstrated the two-way QCS scheme over a 50-km-long fiber, achieving a measured clock difference uncertainty of 3 ps and a time deviation (TDEV) of 60 fs with an average time of 25600 s [25]. However, the cost prohibitively will be increased while extending the two-way scheme to multi-user QCS networks.

In the HOM interferometer-based QCS scheme, the third party distributes entangled photons to distant users and performs the HOM interferometer measurement on the photon pairs back from users, whose results are used to control the adjustable fiber delay to ensure the same propagation time of photons toward users' clocks in real-time transmission [27, 29]. In 2021, Xie M. et al. demonstrated this QCS scheme over a 22-km-long fiber, resulting in a measured clock difference uncertainty of 4 ps and TDEV of 150 fs at an average time of 5500 s [26]. Nevertheless, the critical requirement of equal propagation paths from the third party to users makes this scheme hard to implement in multi-user QCS networks.

In 2022, Lee J. et al. presented a round-trip QCS scheme based on bi-directionally propagating photons generated in a single spontaneous parametric down-conversion (SPDC) source, where the round-trip propagation time can be derived from photons reflected off the end face of the fiber without additional optics [24], resulting a TDEV of 88 ps in 100 s over a 10-km-long fiber. Due to the limited reflection ratio ($\sim 3.5\%$), this scheme has to be improved while extending to long-distance multi-user QCS networks.

In this paper, we propose a multi-user round-trip QCS scheme in the quantum entanglement distribution network, which can be implemented with one single entangled photon source placed at the server. The server distributes the entangled photons to remote multiple users with the WDM strategy, and each user feeds partially received photons back to the server. The clock difference between the server and each user is derived from the one-way and round-trip propagation times, which are determined according to the correlation of entangled photons. Afterward, we demonstrate the multi-user round-trip QCS scheme between the server and a user over a 75-km-long fiber link for approximately 35.6 hours with the frequency dispersion compensation. The experimental results show the clock difference uncertainty is 4.45 ps and the TDEV achieves 426 fs over an average time of 4000 s. Furthermore, our proposed multi-user round-trip QCS scheme is performed with one single entangled photon source and is linearly scalable to many users, with respect to the hardware and deployed fibers.

2 Multi-user round-trip QCS scheme

As the communication infrastructure, the quantum entanglement distribution network has the potential to provide high-precision quantum clock synchronization (QCS) for multiple distant users. In this article, we propose a multi-user round-trip QCS scheme, which can be performed with one single polarization-entangled source and the wavelength division multiplexing (WDM) strategy, illustrated in Fig. 1.

In the multi-user QCS network, the polarization-entangled photon source is located at the server, which generates the photons from the nondegenerate spontaneous parametric down-conversion (SPDC) as

$$|\Phi^+\rangle = \frac{1}{\sqrt{2}}\big(|H_iH_s\rangle + |V_iV_s\rangle\big). \tag{1}$$

According to the energy conservation during the SPDC process, the frequency (f_s and f_i) of two entangled photons satisfies

$$f_p = f_s + f_i, \tag{2}$$

f_p is the frequency of pump photons. Therefore, the entangled signal and idler photons can be separated by demultiplexing equipment such as a dense wavelength division multiplexer (DWDM) or a wavelength selective switch.

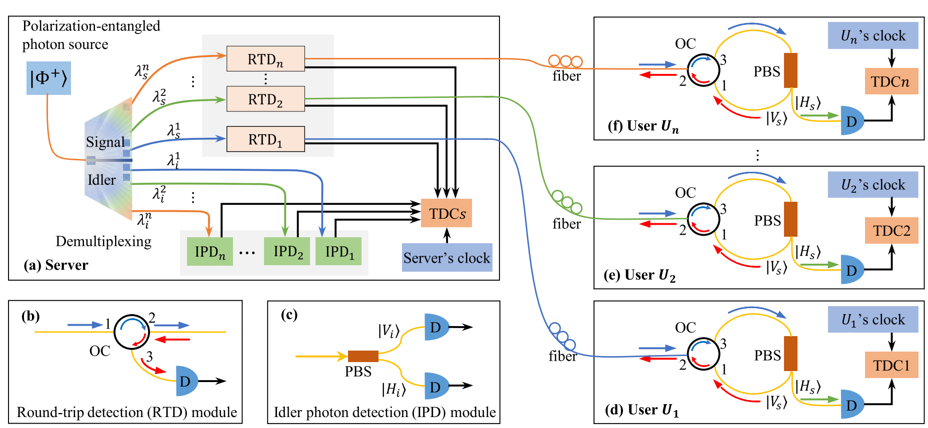

Figure 1 The diagram of the multi-user round-trip QCS scheme in the quantum entanglement distribution network. (a) A demultiplexing equipment separates the entangled signal (idler) photons with the wavelength λ_s^j and λ_i^j for user U_j, $j \in [1, n]$. The signal photons are transmitted to the user, after passing through a round-trip detection (RTD) module. The idler photons are detected in the idler photon detection (IPD) module. (b) RTD module: the input photons pass through an optical circulator (OC) from port 1 to port 2 and the round-trip photons are detected by a detector. (c) IPD module: the entangled idler photons pass through a polarizing beam splitter (PBS), whose output photons $|V_i\rangle$ and $|H_i\rangle$ are detected, respectively. (d), (e) and (f) show the optical path of user U_1, U_2 and U_n, respectively. The input single photons pass through an OC (from port 2 to port 3) and a PBS, which outputs photons $|H_s\rangle$ and $|V_s\rangle$. The $|H_s\rangle$ photons are detected directly and the $|V_s\rangle$ photons are sent back to the server through port 1 to port 2 of the OC. The server's and user's detectors are connected to their respective time-to-digital converters (TDC), which are synchronized by their local clocks

Assuming the separated wavelengths of the entangled photons are λ_s^j (signal) and λ_i^j (idler), $j \in [1, n]$. The entangled signal photons with the wavelength of λ_s^j are transmitted to user U_j through the round-trip detection (RTD) module RTD_j. The corresponding idler photons (wavelength of λ_i^j) are detected by the idler photon detection (IPD) module IPD_j. Here, we present the clock synchronization procedure between the user (U_1) and the server in detail as an example.

For the server, the idler photons with the wavelength of λ_i^1 are transmitted to IPD_1. In IPD_1, the photons are measured by a polarizing beam splitter (PBS), whose output photons $|H_i\rangle$ and $|V_i\rangle$ are detected by two detectors, respectively. The signal photons with the wavelength of λ_s^1 are transmitted to RTD_1. In RTD_1, the photons pass through the optical circulator (OC) from port 1 to port 2, and the round-trip photons from U_1 then go through the OC from port 2 to port 3 and are detected by a detector. The outputs of the detectors are all connected to a time-to-digital converter (TDC*s*) that is synchronized to the server's clocks.

When user U_1 receives the entangled signal photons from the server, the photons pass through OC from port 2 to port 3. Subsequently, the photons are measured by a PBS, and the output $|H_s\rangle$ photons are detected by a detector. The output $|V_s\rangle$ photons are sent back to the server from port 1 to port 2 of OC. The output of U_1's detector is connected to TDC1, which is synchronized to U_1's clock.

Since the photon pairs emerging from the SPDC are time-correlated [30], the time difference between the signal and idler photons can be determined according to the second-order correlation function $G^{(2)}(\tau)$ [31]. Assuming that the clock difference between U_1 and the server is Δt_1, the recorded time of photon $|V_i\rangle$, $|H_i\rangle$, $|V_s\rangle$, $|H_s\rangle$ is t_1, t_2, t_3, t_4.

The time difference τ_{s-u} between $|H_i\rangle$ and $|H_s\rangle$ contains the photon propagation time Δt_{s-u} from the server to the user U_1 and the clock difference Δt_1, which can be expressed as

$$\tau_{s-u} = t_4 - t_2 = \Delta t_{s-u} + \Delta t_1. \tag{3}$$

Similarly, the time difference Δt_{s-u-s} between $|V_i\rangle$ and $|V_s\rangle$ contains the photon propagation time from the server to U_1 and from U_1 to the server, which can be calculated as

$$\tau_{s-u-s} = t_3 - t_1 = \Delta t_{s-u-s}. \tag{4}$$

When the asymmetric delay attack [19] is not conducted, the photon propagation time from the server to U_1 is usually the same as the propagation time from U_1 to the server. Hence, τ_{s-u-s} can be represented as

$$\Delta t_{s-u-s} = 2\Delta t_{s-u}. \tag{5}$$

Therefore, the clock difference Δt_1 can be calculated as

$$\Delta t_1 = \tau_{s-u} - \frac{\tau_{s-u-s}}{2}. \tag{6}$$

The clock difference Δt_j between user U_j and the server can be calculated using the above method, where $j \in [1, n]$. Moreover, the time difference between any pair of users

U_j and U_k can be calculated as

$$\Delta t_{j-k} = \Delta t_j - \Delta t_k, \tag{7}$$

where $j, k \in [1, n]$.

3 Experimental setup

As for the users in our scheme are equivalent, we conducted an experiment demonstration of the proposed scheme over a 75 km fiber with one user and the server. The experimental setup is shown in Fig. 2.

At the server, a continuous wave polarization-entangled photon pair source is used to generate the entangled photons. The source begins with a continuous wave laser emitting light at a wavelength of 775.06 nm in the vertical polarization state $|V\rangle$. The $|V\rangle$ polarization state is rotated by 45° to become the diagonal polarization state $|D\rangle$ by passing through a half-wave plate. Then, the $|D\rangle$ light is reflected by a dichroic mirror (DM) and directed towards a PBS in a Sagnac loop [32].

The PBS outputs $|H\rangle$ and $|V\rangle$ polarized photons in two different directions, respectively. The $|H\rangle$ polarized photon is rotated to $|V\rangle$ polarized photon by a half-wave plate (HWP) before being injected into a 4 cm-long magnesium oxide-doped periodically poled lithium niobate (MgO:PPLN) crystal. The MgO:PPLN crystal has a poling period of 19.5 μm, which facilitates the SPDC process. The SPDC process generates two entangled photons with orthogonal polarizations: a signal photon $|V_s\rangle$ and an idler photon $|V_i\rangle$. After the SPDC generation, one direction $|V_s\rangle|V_i\rangle$ are rotated to $|H_s\rangle|H_i\rangle$ by passing through the HWP. And the generated photons in two directions are combined at the PBS. The entangled photon pair is separated from the pump 775.06 nm light by the DM, and the central wavelength of the entangled photons is 1550.12 nm, corresponding to the center of International Telecommunication Union's (ITU, 100 GHz) channel 34.

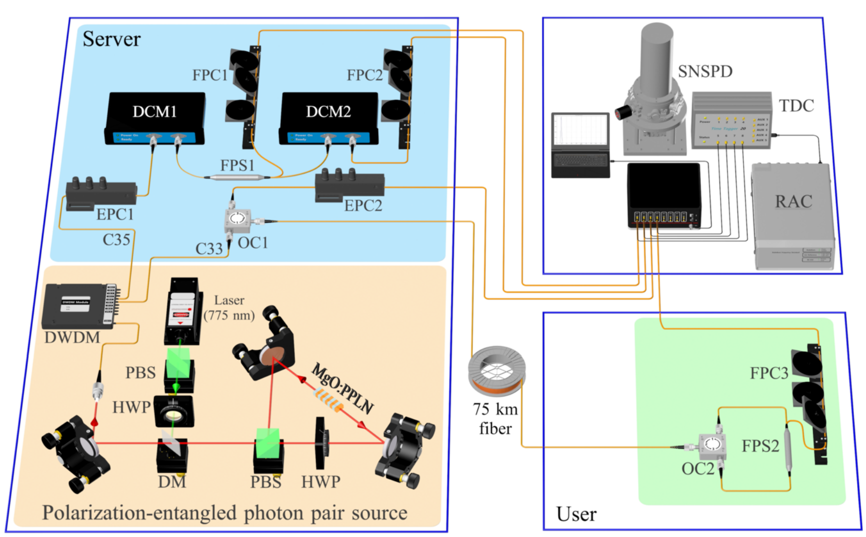

Figure 2 Illustration of the 75 km one-user round-trip QCS experiment. DM: dichroic mirror, HWP: half-wave plate, FPS: fiber polarizing beam splitter, FPC: fiber polarization controller, EPC: electrically driven fiber polarization controller, DCM: dispersion compensation module, DWDM: dense wavelength division multiplexer, SNSPD: superconducting nanowire single-photon detector, RAC: rubidium atomic clock

Then, the signal and entangled idler photons are extracted from ITU C33 (centered at 1549.32 nm) and C35 (centered at 1550.92 nm) by a DWDM. The entangled idler photons first pass through a dispersion compensation module (DCM1), and then are measured by a fiber polarizing beam splitter (FPS1). One output ($|H_s\rangle$) of FPS1 is connected to DCM2 and the $|H_s\rangle$ photons are detected in channel 1 of a superconducting nanowire single-photon detector (SNSPD). Another output ($|V_s\rangle$) photons are detected in channel 2 of SNSPD. The entangled signal photons are sent to the user through the round-trip path with OC1 and OC2, detailly shown in Sect. 2. The user measures the received photons with a fiber polarizing beam splitter (FPS2). The output $|H_i\rangle$ photons are detected in channel 4 of SNSPD and the output $|V_i\rangle$ photons are fed back to the server through the round-trip path. The server detects the round-trip $|V_i\rangle$ photons in channel 3 of SNSPD. And the outputs of SNSPD are connected to a TDC. Furthermore, to compensate for time jitters caused by the crystal oscillator during the photon transmission time, a rubidium atomic clock (RAC) is used to stabilize the TDC clock.

Additionally, three polarization controllers are employed before channels 1, 2, and 4 of the SNSPD, as the detection efficiency of the SNSPD is sensitive to the polarization of photons. To actively compensate for polarization drifting caused by environmental noise, two electrically driven fiber polarization controllers (EPC1 and EPC2) are placed before DCM1 and channel 3 of the SNSPD.

During the experiment, the entangled photon source has a brightness of approximately 3.2×10^6 cps. The insertion loss of both the OC and EPC is about 0.7 dB, and the transmission loss of the 75 km fiber is 15 dB. The SNSPD has a detection efficiency of 80% with a time jitter of 110 ps, and the jitter of TDC is approximately 8 ps. DCM1 and DCM2 are both set to a compensation value of -1230 ps/nm, with an insertion loss of 4 dB.

4 Results and discussion

In the round-trip QCS experiment demonstration, two scenario are considered: one with dispersion compensation (DC) and one without DC. The experiment with DC was carried out for a duration of 35.6 hours, and the experiment without DC was conducted for 28.8 hours. In the experiment without DC, the compensation values of DCMs were set to 0.

During the experiment, correlation analysis is performed based on the arriving timestamps of $|H_s\rangle$, $|H_i\rangle$, $|V_s\rangle$ and $|V_i\rangle$, and generate the coincidence count histograms denoted by $G^{(2)}(\tau_{s-u})$ and $G^{(2)}(\tau_{s-u-s})$. The histograms are then Gaussian-fitted to determine the standard deviations and the expectation values of time differences τ_{s-u} and τ_{s-u-s}.

As an example, Fig. 3 shows the coincidence histograms and the Gaussian-fitted results during the first 100 s experiments. In the experiment without DC, the standard deviations of $G^{(2)}(\tau_{s-u})$ and $G^{(2)}(\tau_{s-u-s})$ are approximately 284 ps and 544 ps, with a total coincidence count of 212.5 kcps and 4.5 kcps, respectively. In contrast, when compensating for the fiber frequency dispersion, the standard deviations are reduced to 174 ps and 201 ps for $G^{(2)}(\tau_{s-u})$ and $G^{(2)}(\tau_{s-u-s})$, respectively, with a total coincidence count of 171.0 kcps and 3.35 kcps. The reduction in the standard deviation indicates a narrower coincidence peak, resulting in the higher precision time difference. However, it should be noted that the increase in the absolute value of DCM results in an increase of the insertion loss, which reduces the coincidence count. In addition, the mathematical expectations of τ_{s-u} and τ_{s-u-s} are calculated from the fitted results as $\tau_{s-u} = -359{,}792{,}659$ ps and $\tau_{s-u-s} = -719{,}587{,}252$ ps (with DC) and $\tau_{s-u} = -359{,}816{,}132$ ps and $\tau_{s-u-s} = -719{,}634{,}126$ ps (without DC).

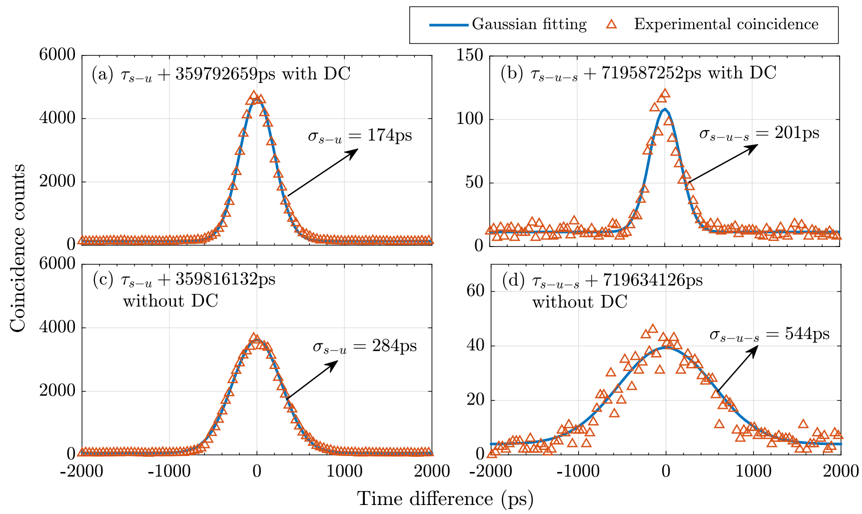

Figure 3 The coincidence count histograms of $G^{(2)}(\tau_{s-u})$ and $G^{(2)}(\tau_{s-u-s})$ in the first 100 s experiment. (a) and (b) [(c) and (d)] show the coincidence histograms $G^{(2)}(\tau_{s-u})$ and $G^{(2)}(\tau_{s-u-s})$ with [without] DC

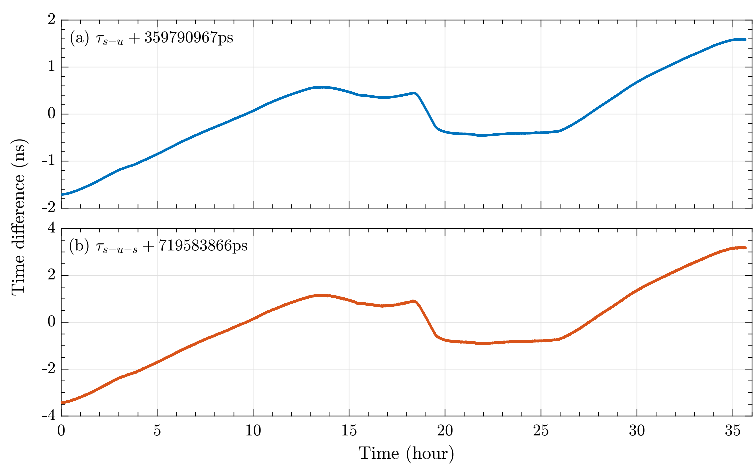

Figure 4 The measured time differences in the experiment with DC. (a) and (b) shows the measured time difference τ_{s-u} and τ_{s-u-s} with the interval time of 20 s, respectively

During the experiment, the time differences τ_{s-u} and τ_{s-u-s} are obtained at intervals of 20 s, to ensure the real-time performance of the system. The calculated τ_{s-u} and τ_{s-u-s} in the experiment with DC are shown in Fig. 4. τ_{s-u} exhibited a variation of approximately 3.36 ns, caused by the experimental noise, such as the temperature fluctuations. In contrast, the time difference τ_{s-u-s} varied twice as fast as τ_{s-u}, with a variation of approximately 6.72 ns during the experiment.

The clock difference Δt is calculated from the time differences τ_{s-u} and τ_{s-u-s} using Eq. (6). For the experiments with and without DC, the mean value of the calculated clock differences is 965.54 ps and 939.95 ps, respectively. The non-zero value of Δt is due to the asymmetric transmission times through various system components such as FPS, OC, DCM, PC, EPC, etc. Additionally, the time offset between the two experimental results is

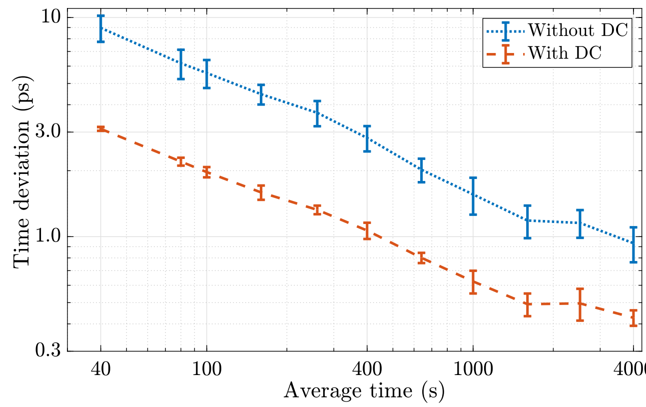

Figure 5 The TDEV of the measured clock differences in the round-trip QCS experiment

attributed to time drifts in the SNSPD, which are affected by the count rate in each channel [33].

In the experiment, the clock difference Δt of each interval is calculated and a clock difference set $S = \{\Delta t_0, \Delta t_1, \ldots, \Delta t_{n-1}\}$ is generated. Then, the standard deviation of these Δt is calculated as 4.45 ps (12.46 ps) for the experiment with (without) DC. The TDEV [34] of the clock difference is calculated as

$$TDEV(m,S) = \sqrt{\frac{1}{6m^2(n-3m+1)} \sum_{j=1}^{n-3m+1} \left(\sum_{i=j}^{m+j-1} \Delta t_{i+2m} - 2\Delta t_{i+m} + \Delta t_i \right)^2}, \tag{8}$$

m means the averaging time contains m intervals. In the TDEV calculation, the averaging time is from 40 s to 4000 s, and the values obtained are shown in Fig. 5. As the averaging time increases to 4000 s, the TDEV is reduced to 426 fs (933 fs) for the experiment with (without) DC.

The experimental results demonstrate the effectiveness of the proposed QCS scheme in achieving high-precision clock synchronization for one user. The same procedure can be applied to synchronize the clocks of other users using other wavelength channels of entangled photons, as the QCS scheme is independent to the wavelengths and optical paths. Moreover, the use of the WDM strategy effectively reduces the spectrum width, leading to high precision even without dispersion compensation, albeit slightly lower than the case with DC.

5 Conclusion

In this paper, we proposed a multi-user round-trip quantum clock synchronization scheme in the quantum entanglement distribution network, which can be implemented with an entangled photon source located at the server. The server distributes the entangled photons to multiple users with the wavelength division multiplexing strategy, and the users feed partial received photons back to the server. Then, the clock difference between the server and each user is calculated from the one-way and round-trip time differences, which are determined according to the time correlation of the entangled photons. In addition, a single-user experiment demonstration was conducted with a 75 km fiber for a duration of 35.6 hours, achieving an uncertainty of 4.45 ps in the measured clock difference and a minimum time deviation of 426 fs at an average time of 4000 s. Furthermore, our proposed scheme can be performed with a single entangled photon source and can scale linearly with respect to the hardware and deployed fibers.

Funding
This work is supported by the National Natural Science Foundation of China under Grant No. 12033007, No. 61875205 and No. 61972410; the Research Plan of National University of Defense Technology under Grant No. ZK19-13, No. 19-QNCXJ-107; Natural Science Foundation of Hunan Province, China under Grant No. 2022JJ40552.

Availability of data and materials
Simulations and scripts are made available upon request by the corresponding author BL.

Declarations

Competing interests
The authors declare no competing interests.

Author contributions
B.L. proposed the scheme. B.Y.T. and M.T. designed, performed the experiment, and contributed equally. This work was supervised by B.L. and W.R.Y., and co-supervised by B.X. and R.F.D. H.C., H.H., H.Z. and S.C.L. contributed to the data collection and analysis. B.Y.T., M.T. and B.L. wrote the draft and all authors reviewed the manuscript.

Author details
[1]College of Advanced Interdisciplinary Studies, National University of Defense Technology, Changsha, China. [2]Strategic Assessments and Consultation Institute, Academy of Military Science, Beijing, China. [3]College of Computer, National University of Defense Technology, Changsha, China. [4]College of Sciences, National University of Defense Technology, Changsha, China. [5]National Time Service Center, Chinese Academy of Sciences, Xi'an, China.

Received: 24 July 2023 Accepted: 17 November 2023 Published online: 22 November 2023

References

1. Wehner S, Elkouss D, Hanson R. Quantum Internet: a vision for the road ahead. Science. 2018;362(6412):9288. https://doi.org/10.1126/science.aam9288.
2. Lo H-K, Curty M, Tamaki K. Secure quantum key distribution. Nat Photonics. 2014;8:595. https://doi.org/10.1038/nphoton.2014.149.
3. Long G-L, Deng F-G, Wang C, Li X-H, Wen K, Wang W-Y. Quantum secure direct communication and deterministic secure quantum communication. Front Phys China. 2007;2(3):251–72. https://doi.org/10.1007/s11467-007-0050-3.
4. Giovannetti V, Lloyd S, Maccone L. Quantum-enhanced positioning and clock synchronization. Nature. 2001;412(6845):417–9. https://doi.org/10.1038/35086525.
5. Giovannetti V, Lloyd S, Maccone L. Positioning and clock synchronization through entanglement. Phys Rev A. 2002;65(2):022309. https://doi.org/10.1103/PhysRevA.65.022309.
6. Beals R, Brierley S, Gray O, Harrow AW, Kutin S, Linden N, Shepherd D, Stather M. Efficient distributed quantum computing. Proc R Soc A, Math Phys Eng Sci. 2013;469(2153):20120686. https://doi.org/10.1098/rspa.2012.0686.
7. Zhao S-R, Zhang Y-Z, Liu W-Z, Guan J-Y, Zhang W, Li C-L, Bai B, Li M-H, Liu Y, You L, Zhang J, Fan J, Xu F, Zhang Q, Pan J-W. Field demonstration of distributed quantum sensing without post-selection. Phys Rev X. 2021;11(3):031009. https://doi.org/10.1103/PhysRevX.11.031009.
8. Zhang Z, Zhuang Q. Distributed quantum sensing. Quantum Sci Technol. 2021;6(4):043001. https://doi.org/10.1088/2058-9565/abd4c3.
9. Su X, Wang M, Yan Z, Jia X, Xie C, Peng K. Quantum network based on non-classical light. Sci China Inf Sci. 2020;63(8):180503. https://doi.org/10.1007/s11432-020-2953-y.
10. Sasaki M, Fujiwara M, Ishizuka H, Klaus W, Wakui K, Takeoka M, Miki S, Yamashita T, Wang Z, Tanaka A, Yoshino K, Nambu Y, Takahashi S, Tajima A, Tomita A, Domeki T, Hasegawa T, Sakai Y, Kobayashi H, Asai T, Shimizu K, Tokura T, Tsurumaru T, Matsui M, Honjo T, Tamaki K, Takesue H, Tokura Y, Dynes JF, Dixon AR, Sharpe AW, Yuan ZL, Shields AJ, Uchikoga S, Legré M, Robyr S, Trinkler P, Monat L, Page JB, Ribordy G, Poppe A, Allacher A, Maurhart O, Länger T, Peev M, Zeilinger A. Field test of quantum key distribution in the Tokyo qkd network. Opt Express. 2011;19(11):10387–409. https://doi.org/10.1364/OE.19.010387.
11. Peev M, Pacher C, Alléaume R, Barreiro C, Bouda J, Boxleitner W, Debuisschert T, Diamanti E, Dianati M, Dynes JF, Fasel S, Fossier S, Fürst M, Gautier JD, Gay O, Gisin N, Grangier P, Happe A, Hasani Y, Hentschel M, Hübel H, Humer G, Länger T, Legré M, Lieger R, Lodewyck J, Lorünser T, Lütkenhaus N, Marhold A, Matyus T, Maurhart O, Monat L, Nauerth S, Page JB, Poppe A, Querasser E, Ribordy G, Robyr S, Salvail L, Sharpe AW, Shields AJ, Stucki D, Suda M, Tamas C, Themel T, Thew RT, Thoma Y, Treiber A, Trinkler P, Tualle-Brouri R, Vannel F, Walenta N, Weier H, Weinfurter H, Wimberger I, Yuan ZL, Zbinden H, Zeilinger A, The secoqc quantum key distribution network in Vienna. New J Phys. 2009;11(7):075001. https://doi.org/10.1088/1367-2630/11/7/075001.
12. Chen Y-A, Zhang Q, Chen T-Y, Cai W-Q, Liao S-K, Zhang J, Chen K, Yin J, Ren J-G, Chen Z, Han S-L, Yu Q, Liang K, Zhou F, Yuan X, Zhao M-S, Wang T-Y, Jiang X, Zhang L, Liu W-Y, Li Y, Shen Q, Cao Y, Lu C-Y, Shu R, Wang J-Y, Li L, Liu N-L, Xu F, Wang X-B, Peng C-Z, Pan J-W. An integrated space-to-ground quantum communication network over 4600 kilometres. Nature. 2021;589(7841):214–9. https://doi.org/10.1038/s41586-020-03093-8.

13. Joshi SK, Aktas D, Wengerowsky S, Lončarić M, Neumann SP, Liu B, Scheidl T, Lorenzo GC, Samec V, Kling L, Qiu A, Razavi M, Stipčević M, Rarity JG, Ursin R. A trusted node-free eight-user metropolitan quantum communication network. Sci Adv. 2020;6(36):0959. https://doi.org/10.1126/sciadv.aba0959.
14. Appas F, Baboux F, Amanti MI, Lemaître A, Boitier F, Diamanti E, Ducci S. Flexible entanglement-distribution network with an algaas chip for secure communications. npj Quantum Inf. 2021;7(1):118. https://doi.org/10.1038/s41534-021-00454-7.
15. Fitzke E, Bialowons L, Dolejsky T, Tippmann M, Nikiforov O, Walther T, Wissel F, Gunkel M. Scalable network for simultaneous pairwise quantum key distribution via entanglement-based time-bin coding. PRX Quantum. 2022;3(2):020341. https://doi.org/10.1103/PRXQuantum.3.020341.
16. Liu X, Liu J, Xue R, Wang H, Li H, Feng X, Liu F, Cui K, Wang Z, You L, Huang Y, Zhang W. 40-user fully connected entanglement-based quantum key distribution network without trusted node. PhotoniX. 2022;3(1):2. https://doi.org/10.1186/s43074-022-00048-2.
17. Zhu EY, Corbari C, Gladyshev A, Kazansky PG, Lo H-K, Qian L. Toward a reconfigurable quantum network enabled by a broadband entangled source. J Opt Soc Am B. 2019;36(3):1–6. https://doi.org/10.1364/JOSAB.36.0000B1.
18. Qi Z, Li Y, Huang Y, Feng J, Zheng Y, Chen X. A 15-user quantum secure direct communication network. Light: Sci Appl. 2021;10(1):183. https://doi.org/10.1038/s41377-021-00634-2.
19. Lee J, Shen L, Cerè A, Troupe J, Lamas-Linares A, Kurtsiefer C. Asymmetric delay attack on an entanglement-based bidirectional clock synchronization protocol. Appl Phys Lett. 2019;115(14):141101. https://doi.org/10.1063/1.5121489.
20. Lee J, Shen L, Cerè A, Troupe J, Lamas-Linares A, Kurtsiefer C. Symmetrical clock synchronization with time-correlated photon. pairs. Appl Phys Lett. 2019;114(10):101102. https://doi.org/10.1063/1.5086493.
21. Li B, Hou F, Quan R, Dong R, You L, Li H, Xiang X, Liu T, Zhang S. Nonlocality test of energy-time entanglement via nonlocal dispersion cancellation with nonlocal detection. Phys. Rev. A. 2019;100(5):053803. https://doi.org/10/gr2j44.
22. Lamas-Linares A, Troupe J. Secure quantum clock synchronization. Advances in Photonics of Quantum Computing, Memory, and Communication XI. vol. 10547. p. 59–66. SPIE. https://doi.org/10/gmvfgb. https://www.spiedigitallibrary.org/conference-proceedings-of-spie/10547/105470L/Secure-quantum-clocksynchronization/10.1117/12.2290561.full Accessed 2023-03-29.
23. Hou F, Quan R, Dong R, Xiang X, Li B, Liu T, Yang X, Li H, You L, Wang Z, Zhang S. Fiber-optic two-way quantum time transfer with frequency-entangled pulses. Phys Rev A. 2019;100(2):023849. https://doi.org/10.1103/PhysRevA.100.023849.
24. Lee J, Shen L, Utama AN, Kurtsiefer C. Absolute clock synchronization with a single time-correlated photon pair source over a 10 km optical fibre. Opt Express. 2022;30(11):18530–8. https://doi.org/10.1364/OE.455542.
25. Hong H, Quan R, Xiang X, Xue W, Quan H, Zhao W, Liu Y, Cao M, Liu T, Zhang S, Dong R. Demonstration of 50 km fiber-optic two-way quantum clock synchronization. J Lightwave Technol. 2022. 1–1. https://doi.org/10.1109/JLT.2022.3153655.
26. Xie M, Zhang H, Lin Z, Long G-L. Implementation of a twin-beam state-based clock synchronization system with dispersion-free hom feedback. Opt Express. 2021;29(18):28607–18. https://doi.org/10.1364/OE.434386.
27. Quan R, Dong R, Zhai Y, Hou F, Xiang X, Zhou H, Lv C, Wang Z, You L, Liu T, Zhang S. Simulation and realization of a second-order quantum-interference-based quantum clock synchronization at the femtosecond level. Opt Lett. 2019;44(3):614–7. https://doi.org/10.1364/OL.44.000614.
28. Quan R, Dong R, Xiang X, Li B, Liu T, Zhang S. High-precision nonlocal temporal correlation identification of entangled photon pairs for quantum clock synchronization. Rev Sci Instrum. 2020;91(12):123109. https://doi.org/10.1063/5.0031166.
29. Bahder TB, Golding WM. Clock synchronization based on second-order quantum coherence of entangled photons. AIP Conf Proc. 2004;734(1):395–8. https://doi.org/10.1063/1.1834461.
30. Hong CK, Ou ZY, Mandel L. Measurement of subpicosecond time intervals between two photons by interference. Phys Rev Lett. 1987;59(18):2044–6. https://doi.org/10/d564wh. Accessed 2023-03-29.
31. Glauber RJ. The quantum theory of optical coherence. Phys Rev. 1963;130(6):2529–39. https://doi.org/10.1103/PhysRev.130.2529.
32. Kim T, Fiorentino M, Wong FNC. Phase-stable source of polarization-entangled photons using a polarization Sagnac interferometer. Phys Rev A. 2006;73:012316. https://doi.org/10/bqfmh3.
33. Mueller A, Wollman EE, Korzh B, Beyer AD, Narvaez L, Rogalin R, Spiropulu M, Shaw MD. Time-walk and jitter correction in SNSPDs at high count. rates. Appl Phys Lett. 2023;122(4):044001. https://doi.org/10/gr2n69. Accessed 2023-03-30.
34. Riley W, Howe D. Handbook of frequency stability analysis. Special publication (NIST SP). Gaithersburg: National Institute of Standards and Technology; 2008. https://tsapps.nist.gov/publication/get_pdf.cfm?pub_id=50505.

Publisher's Note